EXPERIMENTAL ANALYSIS AND MODEL VALIDATION OF AN OPAQUE VENTILATED FACADE

F. Peci López*, R.L. Jensen, P. Heiselberg**, M. Ruiz de Adana Santiago*.**

*Departamento de Química-Física y Termodinámica Aplicada – Escuela Politécnica Superior. Universidad de Córdoba,
Campus de Rabanales. Antigua Carretera Nacional IV, km 396.
14014 Córdoba – España
gf1pelof@uco.es
tlf/fax: +034957212236

Department of Civil Engineering, Aalborg University,** Sohngaardsholmsvej 57, DK-9000 Aalborg, Denmark

Abstract:
Natural ventilation is a convenient way of reducing energy consumption in buildings. In this study an experimental module of an opaque ventilated façade (OVF) was built and tested for assessing its potential of supplying free ventilation and air preheating for the building. A numerical model was created and validated against the experimental data. The experimental results showed that the flow rates induced in the façade cavity were due to mixed driving forces: wind and buoyancy. Depending on the weather conditions one of them was the main driving force, or both were of the same order. When the wind force was the main driving force, higher flow rates were found. In these cases buoyancy acted as supporting driving force. When the wind speed was low and buoyancy prevailed lower flow rates were found. Air and surface temperatures were predicted by the numerical model with a better accuracy than flow and energy rates. The model predicts correctly the influence of the wind and buoyancy driving forces. The experimental OVF module showed potential for free ventilation and air preheating, although it depends on weather and geometrical variables. The use of the numerical model using the right parameters was found viable for analyzing the performance of an OVF.

Keywords: Natural ventilation. Opaque ventilated façade. Ventilated façade. Energy Saving.

1. Introduction

The aim of ventilation in buildings is maintaining a healthy and comfortable indoor environment for building occupants. Nowadays, there is an ongoing concern for energy efficiency and reduction of CO_2 emissions in buildings and new ventilation systems are being studying and implemented for accomplishing ventilation requirements while reducing building energy consumption. One way of reducing the ventilation energy consumption is by using systems based on enhanced natural ventilation. Natural ventilation takes advantage of wind and buoyancy forces to ventilate rooms, reducing the use of mechanical means and therefore reducing energy consumption.

Natural ventilation has been traditionally implemented using the normal building openings like windows and doors. However this method presents some inconveniences like noise increase, wind draughts or incorrect user operation. In the last few years one of the most studied alternative ways to ventilate buildings naturally is by using ventilated facades. A ventilated façade is a double skin façade made up of two layers separated by an air gap. The layers can be opaque or transparent. The air gap normally has an inlet opening through which the ambient air comes in, and one or two exhaust openings for returning the air back to the ambient or introducing it into the building. An air flow can be induced naturally through the facade by wind forces or due to thermal buoyancy. Additionally, in sunny days part of the solar radiation absorbed by the facade is transferred to the air in the gap. This heated air can be introduced in the building if it is convenient, thus reducing the heating energy consumption of the building.

Ventilated facades are classified according to several criteria, like the type of ventilation, the partitioning of the cavity or the ventilation modes [1]. The most widely studied and implemented type of double skin facade is the glazed double skin façade. This type of facade has become very popular due to its aesthetically pleasing exterior [2]. However, the use of double glazed facades increases the risk of overheating in the hot season [3]. Moreover, glazed double skin facades are generally more expensive and the maintenance costs are high. To avoid the disadvantages of using a transparent façade in hot climates, an alternative solution could be using opaque ventilated façades (OVF). In an opaque ventilated façade the two layers are opaque and solar radiation is absorbed in the external layer, reducing the overheating risk. Additionally, an opaque ventilated façade can be made up of conventional materials, thus leading to a smaller cost.

Different types of OVF's have been studied in the last few years. In [4] a rainscreen is studied. A rainscreen is basically an OVF where the inlet and outlet openings are always open to the exterior. A multi-storey OVF was assessed in [5] with a scaled experimental model. A combination of photovoltaic panels and a ventilated façade was studied in [6]. In [7], three types of OVF were analyzed to investigate their thermal behavior.

The zonal approach has been used for simulation of ventilated facades in many ventilated façade studies. The zonal approach is less complicated than CFD models and the accuracy is better than in lumped models [8]. A zonal approach model was used in [4] to assess the performance of a rainscreen façade. Another zonal approach software was used in [9] dividing the façade in several zones and assigning a thermal and air flow node for each one. The zonal approach simulation program TRNSYS had been used extensively for studying DSF's as in [10], [11] and [2].

The aim of this study is to assess the heating and ventilation potential of an experimental OVF and to validate a numerical model with the experimental data obtained. An experimental module was built and sensors were installed to monitor the variables needed for the assessment of the ventilation and energy performance. After a measurement campaign the data were post-processed and analyzed. A numerical model was implemented using a zonal approach software and its parameters were adjusted according with the experimental data. Finally the experimental data were compared with the simulations outputs to evaluate the accuracy of the model predictions.

2. Experimental set up

Module description

An experimental opaque ventilated façade module was built and monitored, under real weather conditions, in the Indoor Environmental Engineering Laboratory of the Department of Civil Engineering of the Aalborg University. The module was equipped with sensors for measuring the variables needed to assess its thermal and ventilation performance. Weather data devices were also installed to register the weather conditions during the measurement period. The laboratory building was a one storey building surrounded by other buildings of similar height, and by access roads and trees. The module was attached to the south-west façade which orientation was 126º W. The location of the module was near a building corner. The wind sheltering effect of the own building and other buildings and obstacles was studied through the experimental evaluation of the local pressure coefficient. The module covered a window at the upper part of the wall, which was used to install the ducts for connecting the ventilated air cavity with the indoor space and pass the cables. This window was blinded and insulated after installing the module to prevent air leakages and thermal losses.

The module was made up of a 0.025 m thick wooden plate, a 0.001 m thick completely flat and smooth galvanized steel plate, with a 0.05 m air gap in between. The air gap was closed laterally with a frame of expanded polystyrene panels of 0.15 m thick. The steel plate was screwed to the wooden plate, through the insulation frame, and it was its only support to avoid introducing additional obstacles to the air flow. The overall dimensions of the experimental module are represented in Figure 1 , and the thermophysical properties of the materials used can be seen in Table 1. The module had an inlet opening at the bottom of the steel plate with the same width as the air gap and 0.05 m height. The outlet opening was a hole of the same width as the air gap and 0.15 m height and it was located in the wooden plate at the top of the air gap. This opening was connected with the indoor space through a transition duct, which reduced the cross section of the channel in order to be able to connect a 0.10 m diameter orifice plate for measuring the flow rate.

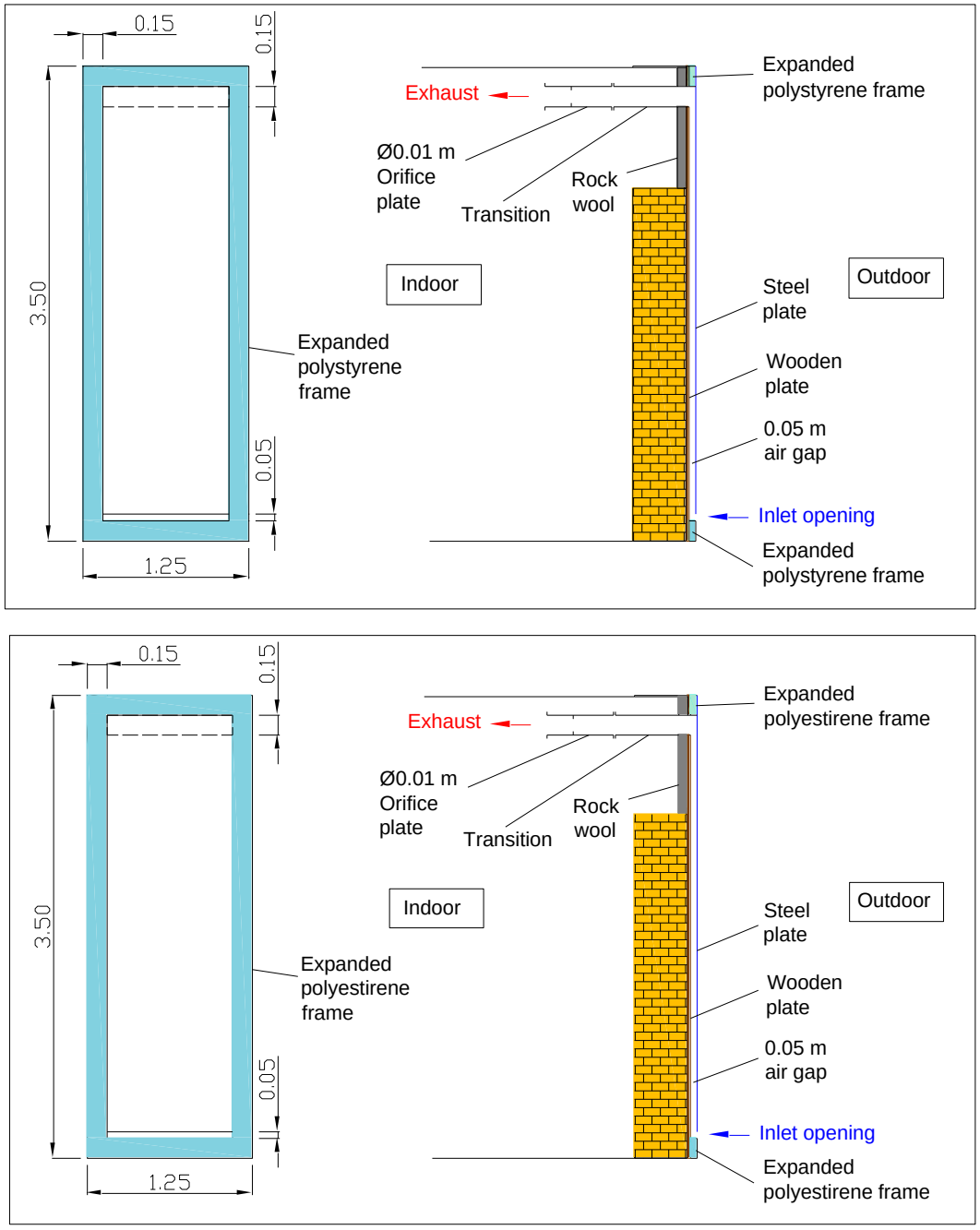

Figure 1. Schematic representation of the experimental OVF module.

Table 1. Thermophysical properties of the materials used in the module of OVF.

Layer	Thickness (m)	Thermal conductivity (W/m K)	Density (kg/m^3)	Specific Heat (J/kg K)
Steel plate	0.001	18	-	-

Air gap	0.05	-	-	-
Wooden plate	0.02	0.14	720	1255

Measurement set up

Weather and thermal variables in the façade were measured in the period from 2nd to 20th of June 2010. Data corresponding to different weather conditions were registered, from sunny warm days to cloudy rainy days. The frequency of measurement was 0.1 Hz. Averaged values were calculated later at 10 min. intervals in order to compare the measurements with the facade model outputs.

Air and surface temperatures inside the façade module were measured in the central axis at five heights using thermocouples type K with accuracy of ±1 ºC. A schematic diagram of the location of the probes is shown in figure 2. The air temperature probes were shielded against long wave radiation with silvered ventilated pipes [12]. Since the steel thermal conductivity was high enough and the plate was very thin, the temperature of the steel plate was supposed to be nearly the same at both sides of the plate. Therefore the steel plate temperature was measured at the inside surface, thus avoiding the solar radiation effects. All surface temperature probes were also protected from long wave radiation with reflective adhesive tape. The room air temperature was also measured using the same method.

Additionally, two horizontal arrays of five thermocouples each were set at two different heights in the air cavity. The aim of these arrays was to measure the temperature profile at the upper and lower part of the air gap for monitoring the air temperature distribution in the cavity and estimating the convection heat transfer coefficient at the inside surfaces of the façade.

An orifice plate was used for measuring the flow rate through the facade. A Ø10 cm diameter was chosen so low flow rates could be measured. For measuring the differential pressure in the orifice a Furness Controls FCO44 0±20 Pa ±2.5% pressure transducer was used. The relative error of flow rate measurements with the orifice plate used was 19%.

The pressure coefficient is an important parameter for modeling the air flow through the façade. This parameter relates the wind speed and direction with the static pressure on a facade opening. It also reflects the effect of the building shape and the urban environment. The pressure coefficient C_p is obtained from the expression:

$$\boldsymbol{P_w = C_P \frac{\rho U^2}{2}} \qquad (1)$$

Where P_w is the pressure differential between static pressure on the façade and atmospheric pressure, ρ is the air density (kg/m^3), and U is the undisturbed wind speed (m/s). Wind speed and direction are typically measured at the roof height of the building. [13].

In order to calculate the pressure coefficient at the inlet opening, three pressure taps were set just below the inlet opening of the module. The average wind pressure differential with respect to the atmospheric pressure was measured. The taps were located far enough to

the opening to prevent the airflow to interfere with the measurement and near enough to be representative of the pressure in the opening [14]. The differential pressure between indoor and outdoor was also measured to obtain an estimation of the internal pressure coefficient. Differential pressure transducers Furness FCO44 0±100 ±2.5% Pa were used.

Two thermocouples were set up at the bottom of the cavity, at both sides of an insulation panel, as shown in Figure 2, in order to estimate the exterior average convection heat transfer coefficient. The heat flux through the insulation panel was evaluated from the two temperature measurements using TRNSYS. Then, the exterior convection coefficient was evaluated through the following expression[15]:

$$\boldsymbol{h = \frac{q_s - q_c + \varepsilon\sigma\left(T_{sky}^4 - T_s^4\right)}{T_s - T_a}} \tag{2}$$

where q_s is the direct solar radiation absorbed by the exterior surfaced, q_c is the heat flux by conduction through the facade, ε is the emissivity of the exterior surface , σ is the Stefan-Boltzmann constant, T_{sky} is the sky effective temperature, T_s is the exterior surface temperature, and T_a is the ambient temperature. The sky effective temperature was approximated by the expression [16]:

$$\boldsymbol{T_{sky} = T_o - 6} \tag{3}$$

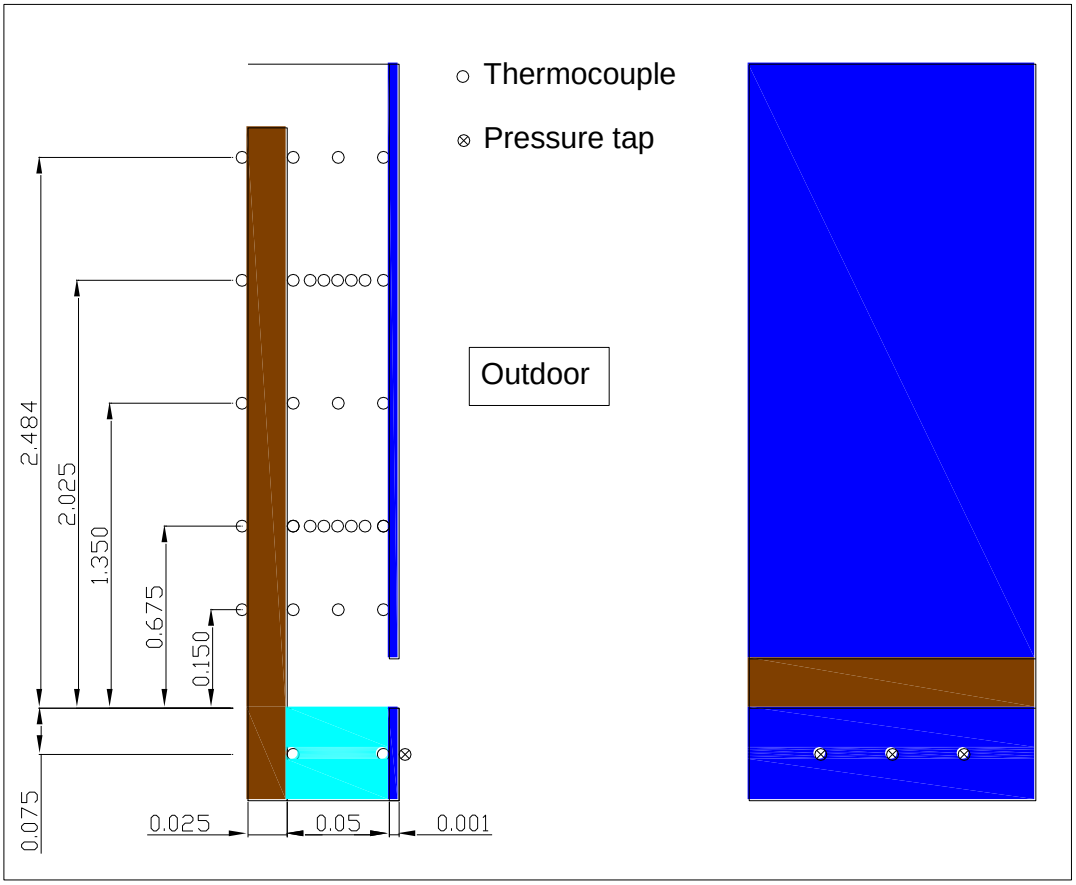

Figure 2. Schematic representation of the positions of sensors in the experimental FVO module. O=thermocouples, X=pressure taps.

Weather variables were also measured. Solar global radiation in the vertical was measured with a Kipp&Zonen pyranometer model CM21 located vertically on the same wall as the experimental module. The local ambient temperature was measured using a shielded thermocouple. Wind speed and direction were measured using an ultrasonic anemometer Gill Windmaster 3D mounted on a10 m mast just in front of the building.

3. Monitoring results

Figure 3 shows the exterior temperature, solar radiation on the vertical and the wind speed and direction during the six days measurement period. The solar irradiation represents the sum of direct solar radiation, diffuse solar radiation and ground and surroundings reflected solar radiation. Days 1 and 5 corresponded to overcast days since maximum solar radiation was less than 400 W/m^2. Days 2, 3 and 4 corresponded to sunny days, and day 6 was a cloudy day although eventually it became sunny after midday. The peak solar radiation on the façade was around 725 W/m^2 without clouds and it oscillates between 70 and 380 W/m^2 for cloudy days. Peak ambient temperatures varied for sunny days from 18 ºC to 24 ºC, whereas in cloudy days the maximum temperatures were around 15ºC.The windiest day was Day 1 with peak values of 9 m/s. The rest of the days the wind velocity

was moderated. The prevalent wind angle was around 300º clockwise from the façade normal.

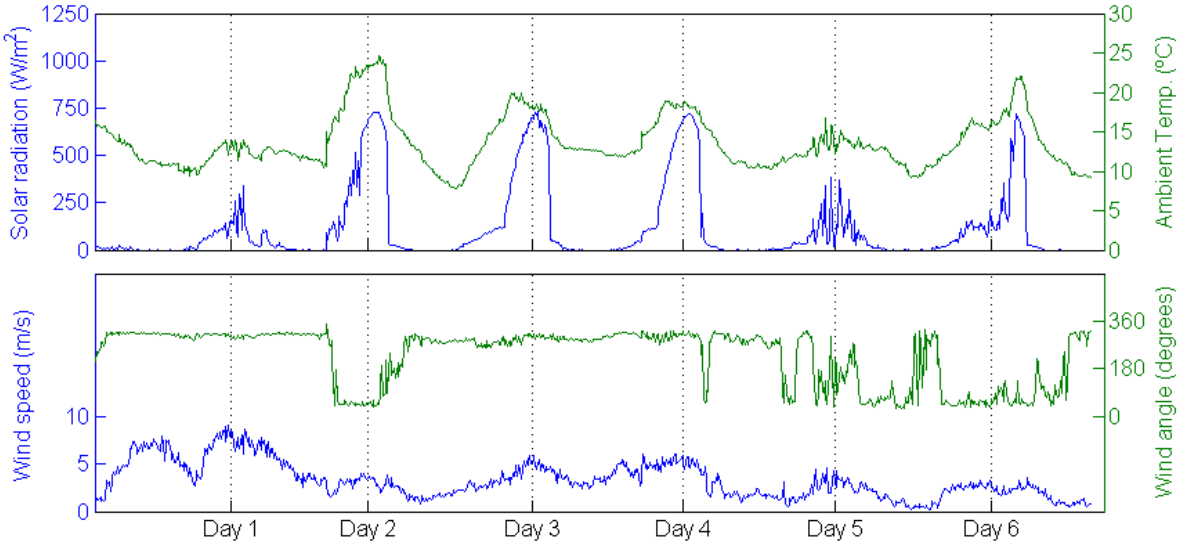

Figure 3. Weather data from the measurement campaign: Solar radiation, ambient temperature, wind speed and direction.

Figure 4Figure 4 shows vertical temperature profiles of the air inside the cavity of the experimental façade module. The profiles represented were measured at the maximum solar radiation point of each day. The measurements were made in the middle point between the cavity walls, so the temperatures don't represent, in principle, the average temperature at that height. However the thermal boundary layer develops quickly and the horizontal temperature profile is quite flat by that height as it can be seen in Figure 5, so these measurements can be considered a good approximation to the average values.

Table 2. Weather conditions and flow rate through the OVF for the peak solar radiation time intervals of the six days of measurements.

	Day 1	*Day 2*	*Day 3*	*Day 4*	*Day 5*	*Day 6*
Solar radiation(W/m2)	341	728	734	720	293	721
Ambient Tempertaure (°C)	14	24	18	18	15	22
Windspeed (m/s)	5.9	2.7	5.2	5.7	3.3	2.3
Flow rate (m3/h)	18.1	10.8	17.7	17.0	6.4	9.6

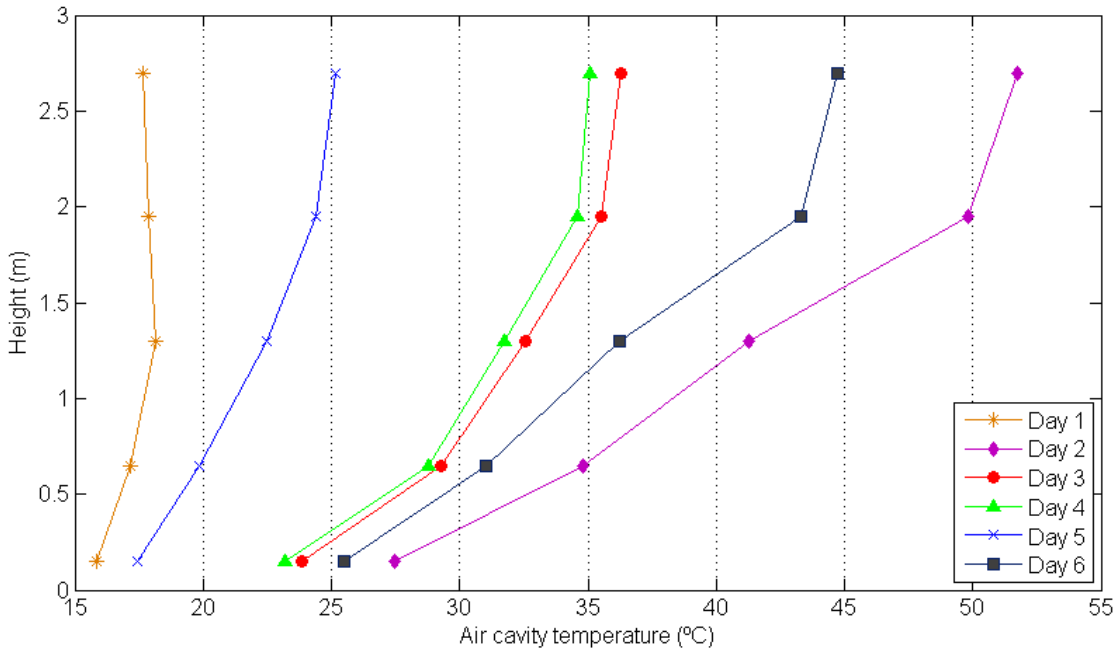

Figure 4. Vertical air temperature profiles in the façade air gap at the point of maximum solar radiation for the six days of measurements.

Figure 5 shows the horizontal temperature profile measured inside the façade module for two different heights. For h=0.63 m, the temperature gradients were negligible near the wooden plate since it was an insulation layer. Nevertheless, in day 2, wooden plate surface was 2 ºC above the air temperature. A possible explanation for this could be that at high temperatures long wave radiation interchange begins to be of the same importance as heat convection, and temperature rises to balance heat transfer.

In the upper part of the cavity, h=2 m, the air temperature profile is practically flat, although there is still a temperature difference of 9ºC between the air next to the steel plate and the steel plate surface. The temperature decline slightly near the wooden plate for all the cases, probably due to the fact that at this height the wooden panel is worse insulated as it was in front of the window hole. Another explanation could be that buoyancy forces become more and more important as temperature rises. This could induce recirculation of air in the upper part of the façade, mixing up hot and warm air and limiting the temperature gradient.

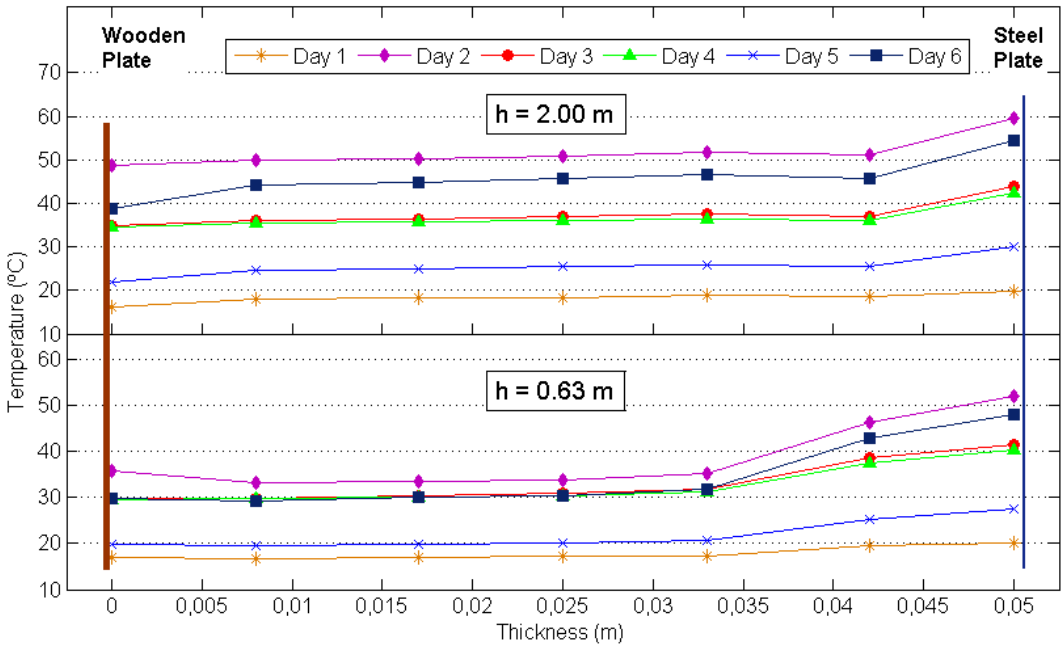

Figure 5. Horizontal temperature profiles of the facade module at two heights for the six days of measurements.

Figure 6 shows the evolution of the horizontal profile at middle height for Day 3. Three stages can be distinguished. During the night the steel plate and cavity air temperature were practically the same whereas the wooden plate surface temperature was higher. At this stage the building was losing energy through the insulation layer as the indoor air temperature was higher than outdoor. When the solar radiation began to raise, a transient stage started in which the steel plate got hotter and hotter until the temperature of the air in the cavity surpassed the wooden plate surface temperature. At this moment the same profiles as shown in figures 4 and 5 remained until the solar radiation started to go down and the inverse transient stage occurred.

In Figure 7 the evolution of cavity air temperatures along the height of the façade is represented. The same temperature stratification as in Figure 4 is maintained all day. Temperature increase began to rise from the sunrise and reached their maximum by 16:30h. It can be seen that the temperature gradient decrease with height.

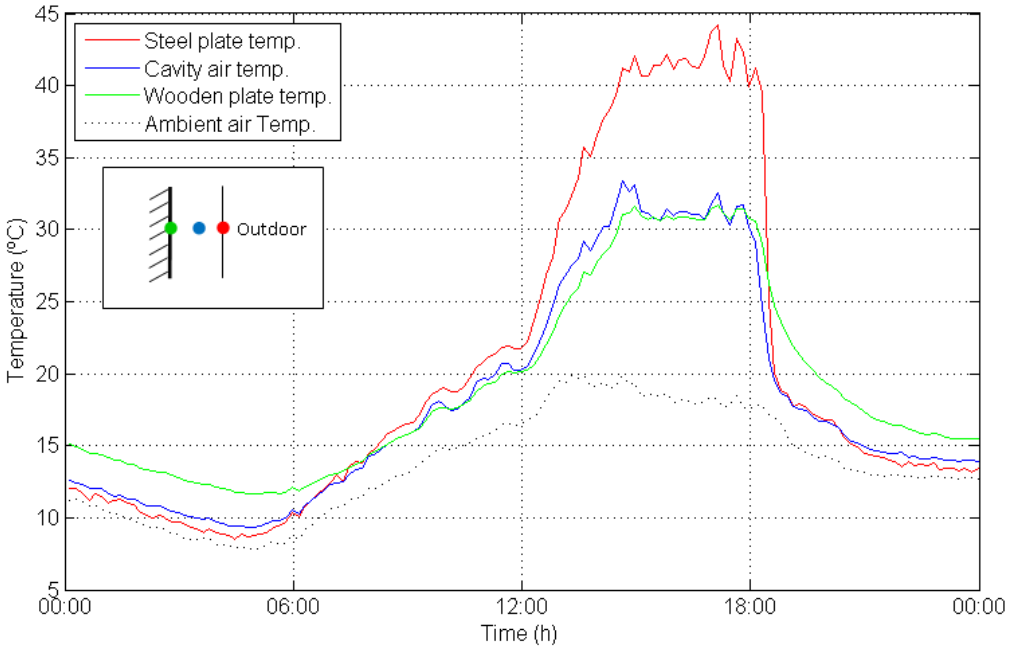

Figure 6. Time evolution of temperatures at the cavity middle height during Day 3.

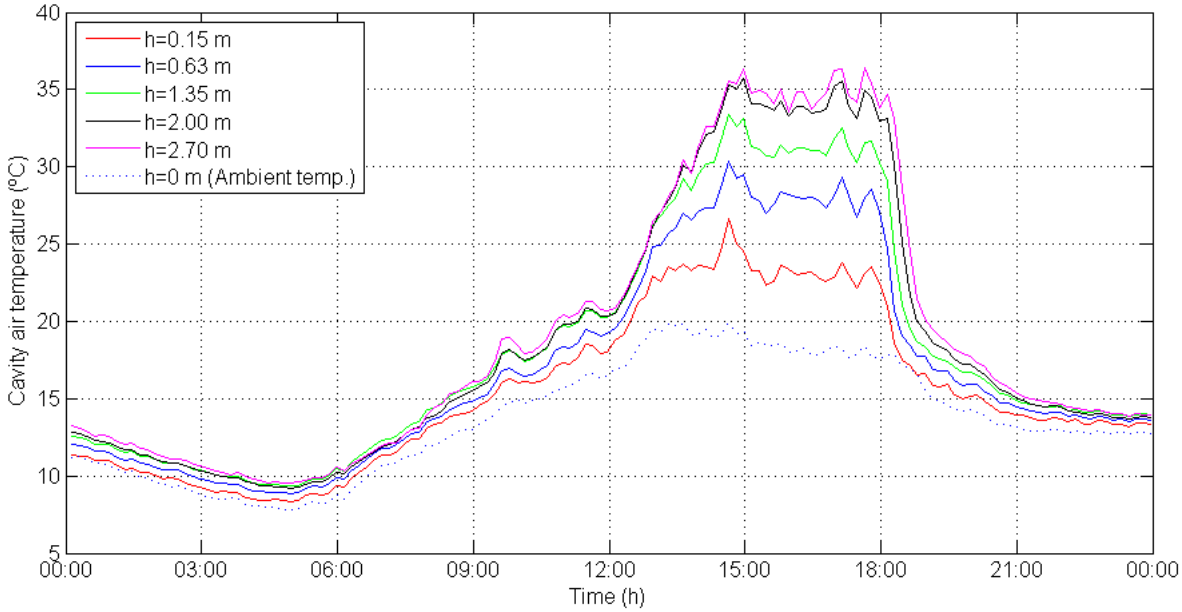

Figure 7. Time evolution of cavity air temperatures along the height of the air gap during Day 3.

4. Model description

A model of the facade module was implemented using the zonal approach building simulation software TRNSYS. The façade air gap was divided into five zones, corresponding to the locations of the temperature probes in the experimental module. The model calculates the temperatures of all zones and the flow rate through them using the weather data file and the model parameter configuration as input data. Therefore a carefully estimation of model parameters had to be done in order to obtain a good approximation to experimental measurements.

The heat transfer modes considered in the model are conduction through solid walls, convection between surfaces and air, long wave radiation interchange between surfaces and solar radiation on external surfaces [17].

The model was based on the zonal energy balance carried out in TRNSYS Type 56 and the airflow network solved by TRNFLOW, which is the integration of the model COMIS in Type 56. In each of the 5 subdivisions of the OVF created the energy transfer by convection and radiation between the zone surfaces, and the energy transported by the airflow coming in and going out the zone are balanced to find the zone air node and surfaces temperatures, and the air flow rate through the OVF. The energy gained by a OVF subdivission air node **i** due to convection in this model can be calculated with the following expression:

$$\dot{Q}_t = \sum \dot{Q}_s + \sum \dot{Q}_f \tag{4}$$

where,

$$\dot{Q}_s = h\, A_j\, (T_j - T_i) \tag{5}$$

is the convection energy transfer from the j surface of the zone, and

$$\dot{Q}_f = \dot{V}\, \rho\, c_p\, (T_k - T_i) \tag{6}$$

are the gains due to air flow from the k previous or next OVF subdivisions.

The energy transfer to a wall due to long wave radiation interchange between surfaces in each OVF subdivision is calculated using the star network described in [17]. The conduction through the walls is solved using the transfer function method by Mitalas, which is also described in [17].

The external long wave radiation interchange was considered through the effective sky temperature. The emissivity of exterior surfaces is fixed at a value of 0.9 in the model. The effective sky temperature had to be modified to account for the lower emissivity of the galvanized steel plate. The indoor temperature measurements were also contained in the

weather data file. The indoor temperature depended of uncontrollable factors so it was considered as a model input.

The thermophysical properties used for heat conduction are shown in table 1. The steel plate layer was modeled as a thermal resistance (R=5.5 x 10^{-5} m^2K / W) due to its small thickness and high thermal conductivity. The properties of all materials used in the experiment were considered constant and evaluated at an average temperature. Radiative properties were taken from standard material property tables.

The OVF channel was modeled as a straight duct. One straight duct was created in the model for each OVF subdivision. The equation for a straight duct is:

$$\dot{m} = A_c \sqrt{\frac{\Delta P \; 2\rho}{\lambda \frac{L}{d} + \zeta}} \tag{7}$$

where A_c is the cross section area of the duct, L is the length of the duct, d is the hydraulic diameter of the duct, ρ is the air density, λ is the friction factor and ζ is the dynamic loss coefficient.

The inlet and outlet OVF openings were modeled as large vertical openings. The mass flow rate can be calculated from the differential pressure with the expression:

$$\dot{m}_{ij} = C_d \int_0^H \sqrt{2\rho(z)\Delta P(z)}\, w \, dz \tag{8}$$

Where $\dot{m}_{ij}$ is the mass flow rate from node i to node j, C_d is the discharge coefficient, ΔP(z) (positive) is the pressure difference between nodes, w is the opening width and H is the opening height. When ΔP(z) is negative, the air flows in the opposite direction and the mass flow rate is calculated evaluating equation (8) changing the sign of ΔP(z).

The pressure difference between two nodes comes from the two air flow driving forces: wind pressure and buoyancy. The wind pressure can be evaluated using equation (1). The pressure difference due to buoyancy between two nodes in a vertical line is evaluated with the following equation:

$$P_i = P_j - g \int_{Z_i}^{Z_j} \rho(z) dz \tag{9}$$

The orifice plate pressure drop curve was used and the pressure loss of the transition duct was measured previously and introduced in the model. The pressure loss in the façade is considered negligible compared with the latter losses at the measured air flow rates.

Convection Coefficients

For heat convection in external surfaces a linear correlation with wind speed has been traditionally used. The wind convection coefficient has been widely studied and a compilation of these correlations is presented in [18]. An average linear correlation as a function of the free stream wind speed V_f was obtained from the experimental measurements:

$$h = 4.8 + 1.7\,V\_f \quad (windward) \tag{10}$$

$$h = 2.6 + 2.5\,V_f \quad (leeward) \tag{11}$$

The convection heat transfer problem in the air cavity can be assimilated to the case of parallel plates with one of the plates insulated and the other with constant heat flux. The average Nusselt number correlations depend on the Reynolds and Prandtl numbers for forced convection and on Rayleigh number for free convection. The flow rates in the air cavity were low, with Reynolds numbers under 1600, so the air flow was always laminar [19]. The prevalence of forced or natural convection was studied through the evaluation of the average Archimedes number, Ar = Gr/Re^2, for each 10 min time interval of maximum solar radiation in Table 2 along the height of the cavity. The Archimedes number represents the ratio of buoyancy forces to inertial forces. When Ar>>1 natural o free convection is dominant, if Ar<<1 it's forced convection and mixed convection in the case of Ar ≈1. As it can be seen in Figure 8, both forced and natural convection were always present in different proportions. Natural convection was of greater importance in the upper part of the cavity as temperatures were higher there. In windy days as days 1, 3 and 4 the Ar number is lower and both effects were of the same order.

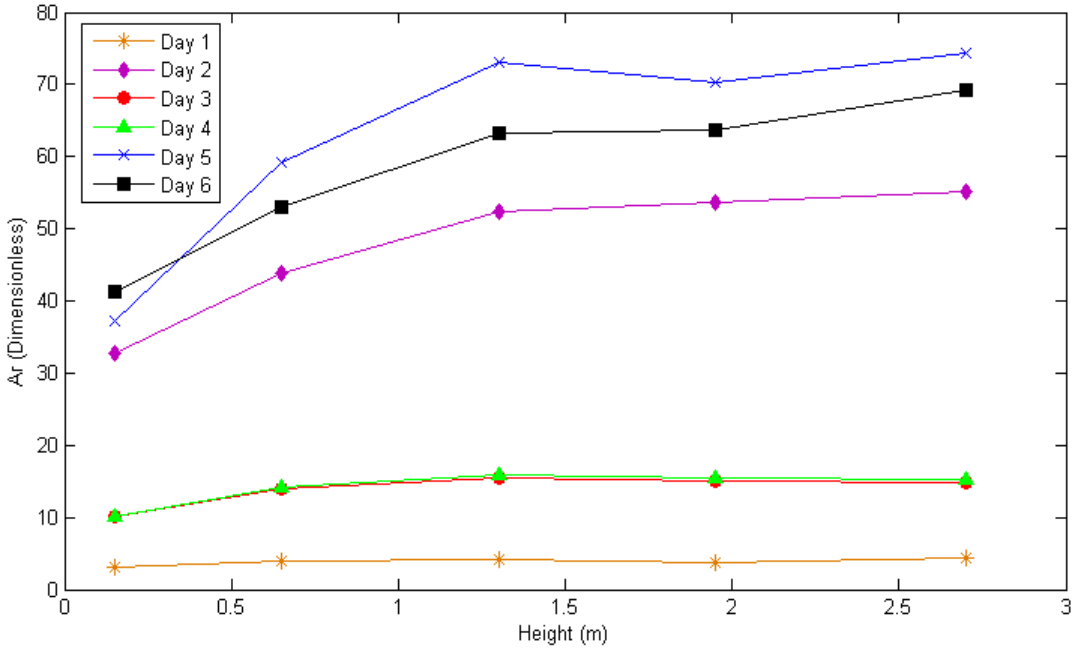

Figure 8. Archimedes number evaluated for the time intervals in Table 2 along the height of the façade cavity.

Using the thermocouples arrays installed in the experimental module, the average convection heat transfer coefficient was estimated by evaluating the temperature gradient near the plate surfaces.

$$Nu_{Dh} = \frac{-D_h \frac{\partial T(x,y)}{\partial y}\Big|_{y=0}}{(T_s - T_a)} \quad (12)$$

Where D_h is the hydraulic diameter of the channel, T_s is the surface temperature and T_a is the average air temperature. An average value of Nu_{Dh}=6.11 was found and this value was used in the numerical model.

Pressure coefficient

Figure 9 represents the average C_P values measured as a function of the wind angle respect to the façade normal. To evaluate the dependency of the averaged C_p with the number of sectors used, the values were averaged for sectors of (360/n)º, with n=8, 12 and 16.

For rectangular buildings without any interference of nearby buildings, positive values of C_P are expected in the windward side for wind angles from 0º to 60º, approximately, and negative values for angles from 60º to 180º [19]. In the experiment, the C_P values obtained were not symmetric with respect to the façade normal direction. For 0º<α<180º C_P values were all negative, because the module was sheltered due to the shape of the building and the presence of nearby buildings. For 180º>α>360º the sheltering effect was smaller as there were no buildings in this direction. Values became positive for 250<α<270º, which was a behavior more similar to that of unsheltered buildings.

The results showed in Figure 9 are similar to those obtained with CFD or wind tunnel measurements for buildings with nearby obstacles [20]. However, It has to be taken into account that the experimental values of C_P showed in Figure 9 are local, and local pressure coefficients decrease with lower heights, so lower values of C_P were expected since the inlet opening was located at the bottom of the wall (Figure 1).

The dependency of averaged C_P values on the number of sectors can be neglected for n>8. In this study eight angles were used in simulations.

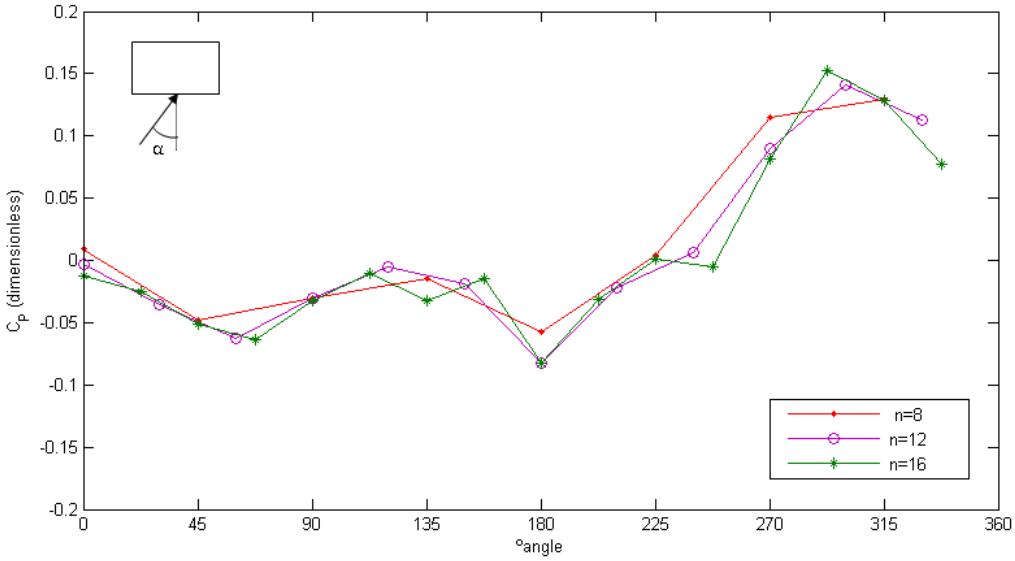

	0º	*45º*	*90º*	*135º*	*180º*	*225º*	*270º*	*315º*
C_p(n=8)	0.001	-0.05	-0.03	-0.015	-0.058	0.0041	0.115	0.1296

Figure 9. Averaged pressure coefficient C_P for divisions of α=360/n.

5. Façade performance and simulation results

In order to validate the performance of the numerical model the most important variables were confronted to the experimental data. The exhaust air temperature and the air flow rate were evaluated, as well as the incoming energy supplied by the airstream.

Figure 10 shows the comparison of the experimental data measurements with the simulation ouput for the air temperature at the top of the façade module. This temperature can be considered the temperature of the air that enters the room. The maximum air temperature registered was over 50 ºC and corresponds to midday of Day 2. Air temperature in Days 3 and 4 didn't get so high temperatures despite having the same solar radiation levels. The reason for this was the higher wind speed during those days. In general the more windy the day was the lower temperatures inside the façade there were. It can be also seen comparing Day 1 and Day 5. Both days were cloudy and with similar levels of solar radiation, however Day 1 outlet air temperatures were lower than temperatures in Day 5. Since heat convection from the steel plate to the ambient air depends linearly on the wind speed, the more windy the day the more heat loss to the ambiente air and the lower steel plate temperatures, and therefore the lower air temperatures. Nevertheless the maximum increment of temperature reached more than 10 ºC for Day 3 and Day 4, as it can be seen in Figure 4.

There aren't many studies for comparing exhaust air temperature in an opaque ventilated façade. Double skin facades performance regarding solar radiation is similar to the results obtained for opaque ventilated facades [21]. In[2] insuficient solar radiation is related to the lower flow rates. Typically temperatures over 40ºC are reached depending on the season. Air temperature also depends on geometry. Average cavity air temperatures decrease with

cavity thickness. However heat loss by convection to the ambient air is lower in transparent façades because the hottest layer, normally the shading device, is inside the cavity and therefore protected from wind. The external layer temperature and hence the air flow temperature is strongly influeced by wind in an opaque ventilated façade.

In order to evaluate the accuracy of the simulation results a linear regression analysis was carried out for the predicted and experimental outlet air temperatures, Figure 11. The bigger errors were found for the higher temperatures, this was also found for other models [8]. The coefficient of determination was 0.9356 and temperatures from simulation showed good agreement with the experimental results.

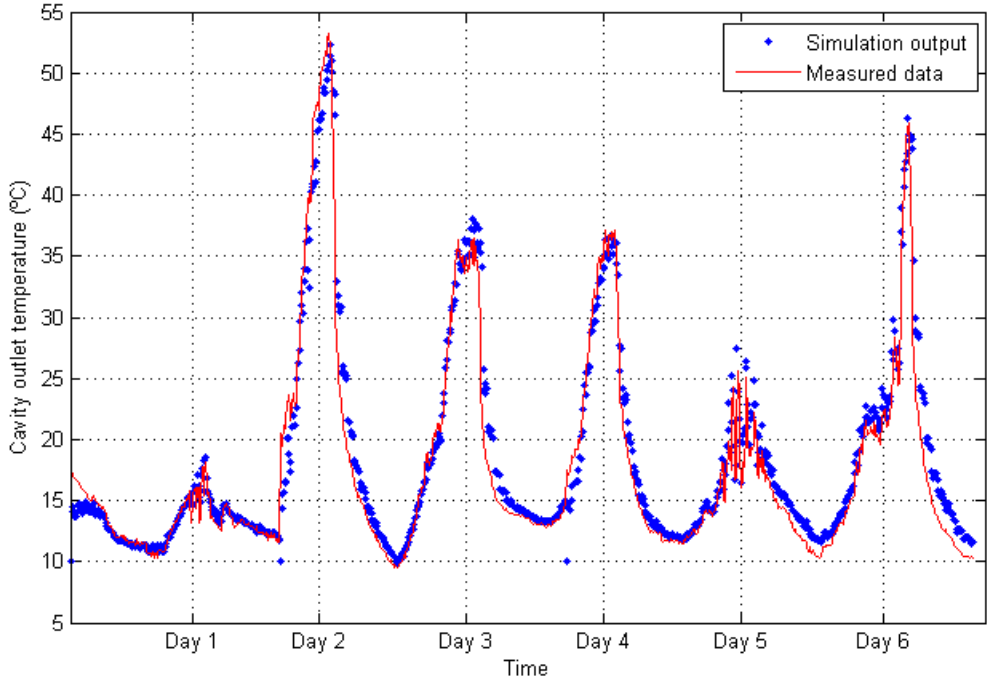

Figure 10. Comparison of exhaust air temperature measured and obtained by simulation

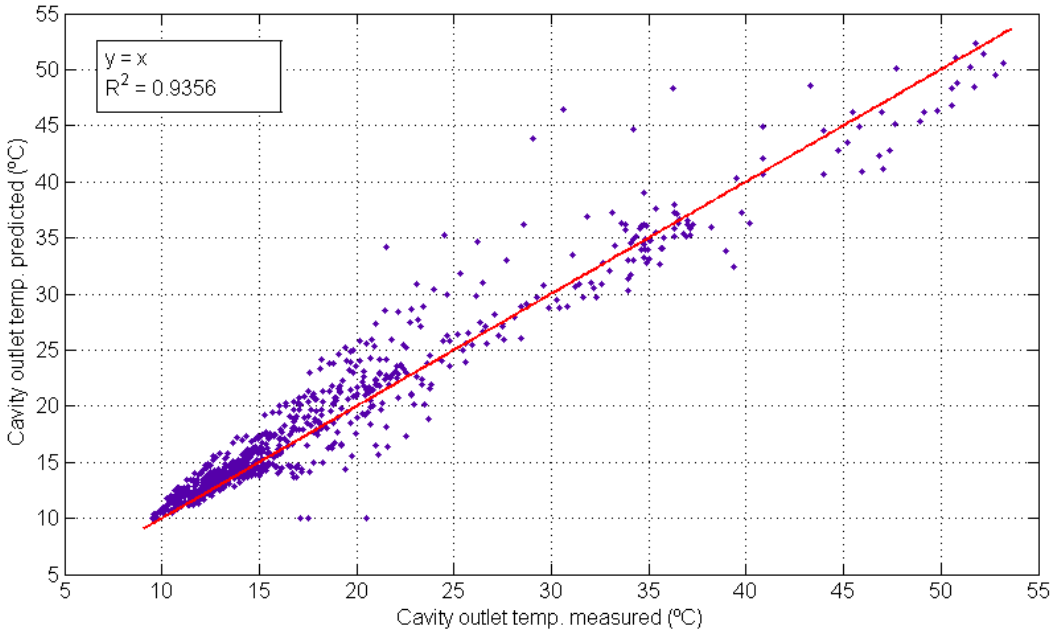

Figure 11. Correlation between exhaust temperature measured and obtained by simulation.

Experimental and simulation results of the air flow rate and energy introduced by the supply air in the room are represented in 3. The range of air flow rate measured was from negative values of – 5 m^3/h (inversed flow) to maximum values over 20 m^3/h. The average air speed in the cavity had a maximum value of 0.15 m/s. The energy introduced with the ventilation air was higher for the sunny days (Days 2, 3 and 4) with peak values of 130 W. On the cloudy days (Days 1,5 and 6) the energy had values under 50 W.

Low temperatures were expected inside the façade for cloudy days. Sunny days presented high temperature increases in general. It is noticeable that the lowest increases corresponded to the windiest days, due to the increase of the external convection coefficient with windspeed. For the same level of solar radiation, Day 1 temperature rose only 2º whereas increment in Day 5 was 7ºC. Ambient temperature also affected the temperature in the cavity. The increment of temperature in Day 2 was higher than in Day 6 despite having the same peak solar radiation. However the ambient temperature was lower in the later. The maximum vertical temperature increase registered was 24ºC in Day 2.

It can be observed a clear correlation between air flow and energy rate and solar radiation, ambient temperature and wind pressure. On Day 1 the prevalent driving force was the wind pressure. On this day the air flow rate had peak values over 10 m^3/h with wind pressure peak values up to 4 Pa and solar radiation under 300 W/m^2. On Days 2 and 6 solar radiation was high and wind pressure was almost non-existent so buoyancy was the main driving force. On days 3 and 4 solar radiation was high and wind pressure had moderate values so driving forces are mixed. With the same solar radiation levels as day 2 the air flow rates for days 3 and 4 were slightly greater due to the support of wind pressure.

The linear regression analysis for the air flow rate and the energy of the air flow can be seen in Figure 12 and Figure 14. Bigger errors were expected in both cases due to the high uncertainty in the air flow rate measurements and the difficulty of adjusting all the parameters that affects the air flow rate calculations. The model tends to overpredict the air preheating energy as it can be seen in Figure 14. However, the model has proven to be sensitive to the main air flow driving forces, as it can be seen in Figure 12. The high flow rates that can be seen in Day 4 are due to some tests carried out using mechanical ventilation for trying to control the indoor pressure, and must not have to be taken into account. They were included to provide a continuous source of data to the model.

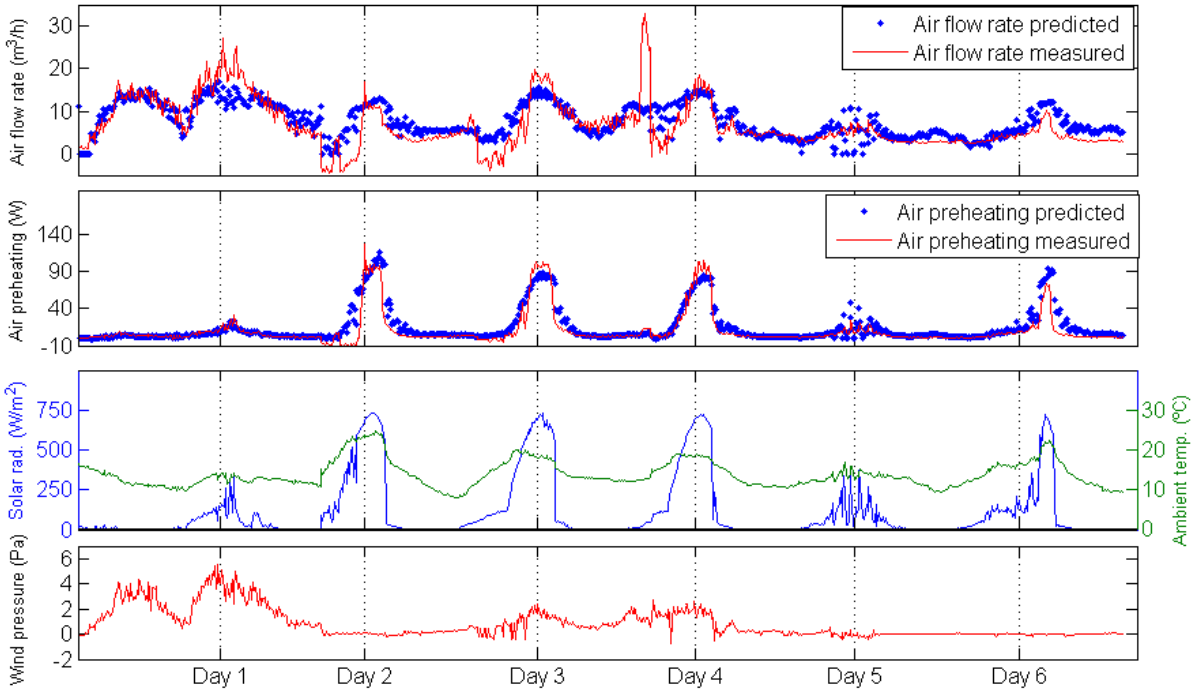

Figure 12. Comparison between air flow rate and energy measured and obtained by simulation.

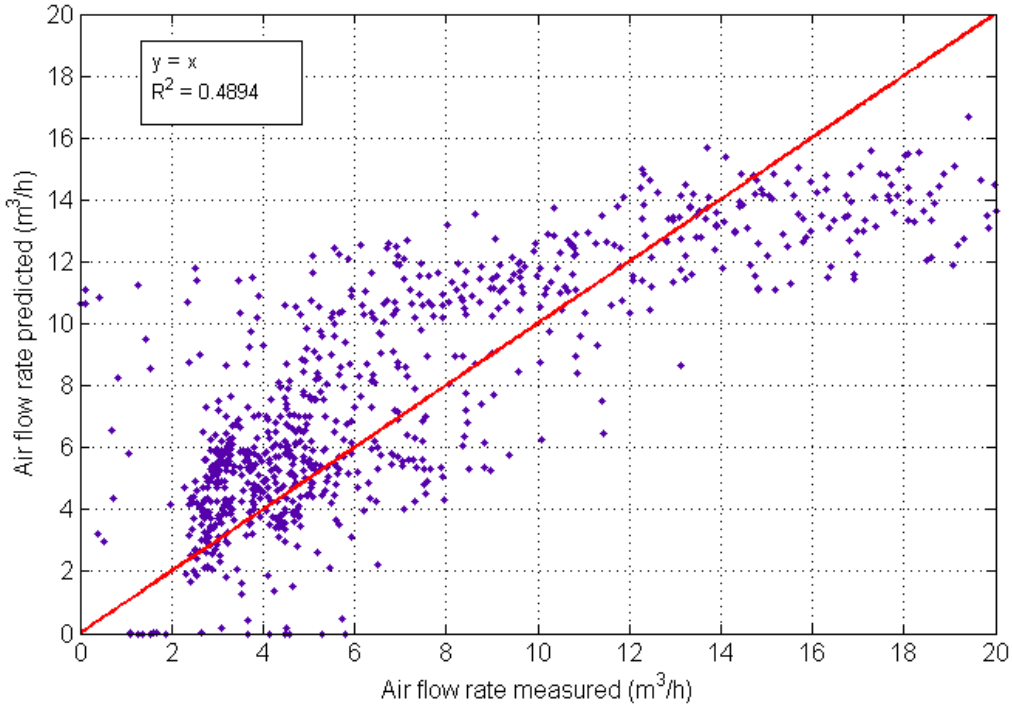

Figure 13. Correlation between air flow rates measured and obtained by simulation.

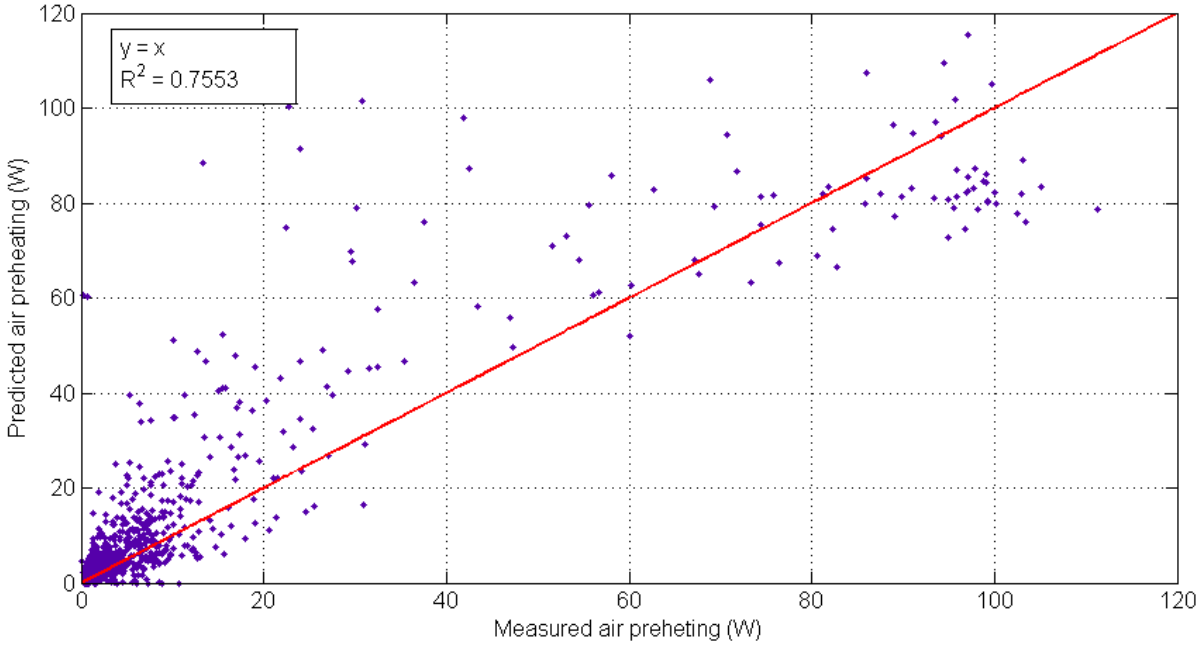

Figure 14. Correlation between energy measured and obtained by simulation.

4 Conclusions

In this paper the performance of an experimental OVF module was assessed and the experimental data were used to validate a numerical model. The main conclusions from this piece of work are now summarised:

- The performance of the facade depends on the meteorological variables. Wind speed and direction and solar radiation are the driving forces of air flow. If the wind speed is the prevalent driving force temperatures are lower and if buoyancy is the main driving force temperatures rise.
- Air flow rates due to wind forces depend on wind speed and direction but also on the Cp values that are characteristic of geometry and location of the building.
- If wind increases the air flow rates, also increases the heat loss due to convection to the ambient air.
- The model created is sensitive to the driving forces of air flow.
- The outputs of simulation had a good agreement with experimental data. Temperatures were well predicted whereas air flow rate has bigger errors.
- Flow conditions in the cavity corresponded with the analysis from experimental data.
- Having the right parameters it's viable to use the model for analyzing the performance of OVF's, although the air preheating capacity of the façade will be in general overpredicted.

5 Acknowledgement

The present study has been realized within the Spanish National Plan for R+D: "Integration of constructive systems of active ventilated facades for ensuring efficient energy consumption and indoor air quality. Implementation on non-residential buildings", Ref. BIA2006-15398-C04-04, Ministry for Science and Education, Government of Spain.

References

[1] Loncour X, Deneyer A, Blasco M, Flamant G, Wouters P. Ventilated Double Facades. Belgian Building Research Institute Department of Building Physics, Indoor Climate & Building Services; 2004.
[2] Kim YM, Kim SY, Shin SW, Sohn JY. Contribution of natural ventilation in a double skin envelope to heating load reduction in winter. Building and Environment. 2009;44:2236-44.
[3] Gratia E, De Herde A. Greenhouse effect in double-skin facade. Energy and Buildings. 2007;39:199-211.
[4] Marinosci C, Strachan PA, Semprini G, Morini GL. Empirical validation and modelling of a naturally ventilated rainscreen facade building. Energy and Buildings. 2011;43:853-63.
[5] Mingotti N, Chenvidyakarn T, Woods AW. The fluid mechanics of the natural ventilation of a narrow-cavity double-skin facade. Building and Environment. 2011;46:807-23.
[6] Mei L, Infield D, Eicker U, Fux V. Thermal modelling of a building with an integrated ventilated PV facade. Energy and Buildings. 2003;35:605-17.
[7] Patania F, Gagliano A, Nocera F, Ferlito A, Galesi A. Thermofluid-dynamic analysis of ventilated facades. Energy and Buildings. 2010;42:1148-55.
[8] Jiru TE, Haghighat F. Modeling ventilated double skin facade - A zonal approach. Energy and Buildings. 2008;40:1567-76.
[9] Chan ALS, Chow TT, Fong KF, Lin Z. Investigation on energy performance of double skin facade in Hong Kong. Energy and Buildings. 2009;41:1135-42.
[10] Haase M, da Silva FM, Amato A. Simulation of ventilated facades in hot and humid climates. Energy and Buildings. 2009;41:361-73.

[11] Kim YM, Lee JH, Kim SM, Kim S. Effects of double skin envelopes on natural ventilation and heating loads in office buildings. Energy and Buildings. 2011;43:2118-26.
[12] Kalyanova, Olena ; Zanghirella, Fabio ; Heiselberg, Per ; Perino, Marco ; Jensen, Rasmus Lund. /Measuring Air Temperature in Glazed Ventilated Facades in the Presence of Direct Solar Radiation.I: Proceedings of Roomvent 2007. red. / Olli Seppänen ; Jorma Säteri. FINVAC ry, 2007.
[13] ASHRAE. Airflow Around Buildings. ASHRAE Handbook-Fundamentals 2005. Chap. 16.
[14] Chiu YH, Etheridge DW. External flow effects on the discharge coefficients of two types of ventilation opening. Journal of Wind Engineering and Industrial Aerodynamics. 2007;95:225-52.
[15] Loveday DL, Taki AH. Convective heat transfer coefficients at a plane surface on a full-scale building facade. International Journal of Heat and Mass Transfer. 1996;39:1729-42.
[16] Duffie JA, Beckman WA. Solar Energy Thermal Process. New York: John Wiley; 1974.
[17] Solar Energy Laboratory UoW-M, GmbH TE, CSTB, TESS. TRNSYS 16 Reference Manual 2004.
[18] Palyvos JA. A survey of wind convection coefficient correlations for building envelope energy systems' modeling. Applied Thermal Engineering. 2008;28:801-8.
[19] Incropera FP, Witt DDD, Bergman TL, Lavine AS. Fundamentals of Heat and Mass Transfer: Wiley; 2006.
[20] Costola D, Blocken B, Hensen JLM. Overview of pressure coefficient data in building energy simulation and airflow network programs. Building and Environment. 2009;44:2027-36.
[21] Zanghirella F, Perino M, Serra V. A numerical model to evaluate the thermal behaviour of active transparent facades. Energy and Buildings. 2011;43:1123-38.